The Oceanic Eddy Heat Transport

Steven R. Jayne

MIT-WHOI Joint Program in Oceanography, Woods Hole Oceanographic Institution, Woods Hole, Massachusetts

Jochem Marotzke

School of Ocean and Earth Science, Southampton Oceanography Centre, Southampton, United Kingdom

Abstract. The rectified eddy heat transport is calculated from a global high-resolution ocean general circulation model. The eddy heat transport is found to be strong in the western boundary currents, the Antarctic Circumpolar Current, and the equatorial region. It is generally weak in the central gyres. It is also found to be largely confined to the upper 1000 meters of the ocean model. The eddy heat transport is separated into its rotational and divergent components. The rotational component of the eddy heat transport is strong in the western boundary currents, while the divergent component is strongest in the equatorial region and Antarctic Circumpolar Current. In the equatorial region, the eddy heat transport is due to tropical instability waves, while in the western boundary currents and the Antarctic Circumpolar Current the large eddy heat transports arise from the meandering of the currents. Stammer's method for estimating the eddy heat transport from an eddy diffusivity derived from mixing length arguments, using altimetry data and the climatological temperature field, is tested and fails to reproduce the model's directly evaluated eddy heat transport in the equatorial regions and the western boundary currents. Possible reasons for the discrepancy are explored. However, in the Antarctic Circumpolar Current region, the model's eddy heat transport is shown to agree well with his estimate.

1. Introduction

The transport of heat by mesoscale eddies in the ocean is the subject of considerable interest and debate, because it is suspected to be an important term in the time-mean ocean heat transport. The eddy heat transport arises from the rectification of velocity and temperature variability, however the fundamental dynamics that underlie the transport are not clear and have not been adequately explained. The role of the oceanic mesoscale eddy field in climate processes has been only marginally addressed observationally in the ocean (Bryden 1979; Bryden and Heath 1985; Bryden and Brady 1989; Stammer 1998; Wunsch 1999). Coarse resolution ocean models, such as those used in climate models, do not resolve the transport processes associated with the oceanic mesoscale field. Therefore, it has been the subject of much speculation and theoretical consideration because of the need to include it as a sub-grid scale parameterization in coarse resolution climate models (*e.g.*, Gent and McWilliams 1990; Holloway 1992; Danabasoglu et al. 1994; Visbeck et al. 1997; Griffies 1998). Tests of these parameterizations have met with some success when applied to atmospheric data (Kushner and Held 1998) and ocean models (Böning et al. 1995; Rix and Willebrand 1996), however, little work has been done to date on investigating characteristics of the eddy heat transport in high-resolution, global ocean circulation models.

Unfortunately, the time-mean eddy heat transport is one of the most poorly observed quantities in the ocean. Wunsch (1999) recently compiled a collection of the available current-meter data in an attempt to assess its magnitude in the ocean. In general, he found it was significant in the western boundary current regions of the Pacific and Atlantic

Submitted to the Journal of Physical Oceanography

Oceans. It was also found to be very small in the interior of the ocean gyres. However, the sparseness of the current meter data precludes any separation into the rotational and divergent components, making the fluxes nearly impossible to interpret. Stammer (1998) recently used satellite altimetry data to compute an eddy diffusivity, which he then combined with a temperature climatology to estimate the eddy heat transport. His results were consistent with the picture that the eddy heat transport is large in the boundary currents and weak in the interior of the gyres. The time-mean eddy heat transport has also been addressed by several regional process studies, some of which will be discussed later (Bryden 1979; Bryden and Heath 1985; Bryden and Brady 1989; Bower and Hogg 1996; Cronin and Watts 1996).

In this paper we explore the characteristics of the rectified eddy heat transport taken from a high-resolution global ocean general circulation model. The eddy heat transport is examined by basin, by depth interval and by dynamical component (Section 2). Then in Section 3, the vector distribution of the rectified eddy transport is considered. Following the suggestion of Marshall and Shutts (1981) it is separated into its rotational and divergent parts with the Gulf Stream as an example. The rotational component can not transport heat across latitude circles and does not contribute to the poleward transport of heat by the oceans, whereas the divergent component of the heat transport does affect the local heat balance and does transport heat northward. It is shown that for a coherent meandering jet, the rotational eddy heat transport dominates and it is not necessarily down gradient, leading one to doubt the validity of claims that current-meter data show down-gradient temperature transport (Section 4). A comparison of the model's northward eddy heat transport and a global estimate derived from TOPEX/POSEIDON data (Stammer 1998) is made. The basic technique used by Stammer (1998) is tested and thereby the assumptions that were used in calculating it are evaluated. Lastly, the eddy heat transport at a few selected locations is examined by using its cospectrum for an indication of what part of the frequency spectrum is contributing to the rectified heat transport (Section 5).

2. General characteristics of the eddy flux

The numerical simulation output we use for this study is from run 4_B of the Parallel Ocean Climate Model (POCM), archived at three day intervals. The POCM is a primitive-equation, level model configured for the global ocean between 75°S and 65°N, with realistic topography (see Jayne and Marotzke 2001, for a discussion of the model's time-varying heat transport). The model has an average resolution of about 1/4° and 20 vertical levels. Previous studies (Stammer et al. 1996; McClean et al. 1997) have shown that the POCM model simulation's eddy energy is too weak by at least a factor of two when compared to the observed ocean. However, it is hoped that while future higher resolution model runs may change the quantitative details presented here, in general the overall qualitative picture would remain similar (as suggested by the analyses of Cox 1985; Beckmann et al. 1994). For example, Beckmann et al. (1994) found in their North Atlantic Ocean model that increasing the resolution did indeed change the eddy heat transport, but that the heat transport by the mean flow was also affected, but when combined there was very little overall change in the heat transport. Therefore, one might expect that increased resolution likely will increase the magnitude of the eddy heat transport, but that its overall structure would be qualitatively similar. However, it remains to be seen whether this will hold true. In part, this work on the rectified eddy heat transport should be regarded as a demonstration of what analyses could be done on higher resolution, and hopefully more realistic, ocean model runs to understand what the dynamics behind the eddy heat transport are.

The time-mean eddy heat transport was calculated from the model output at each grid point using the identity given by:

$$\overline{v'\theta'} = \overline{v\theta} - \overline{v}\,\overline{\theta} \tag{1}$$

where the overbar represents the time-mean and the prime deviations from it. This calculation was performed for both components of the velocity. Here we will consider the northward eddy heat transport in a few different manners: separated by basin, by depth, by dynamical components, and finally as a function of longitude and latitude.

To begin, the zonal integral of the northward eddy heat transport for both the World Ocean and the individual ocean basins are compared to the heat transport by the time-mean circulation in Fig. 1, and then plotted together in Fig. 2. This is similar to the analysis done by Semtner and Chervin (1992) and McCann et al. (1994) on the 1/2° POCM run. The results are remarkably similar to theirs. Notably the eddy transport in the Antarctic Circumpolar Current is higher in the 1/4° run, suggesting that increasing model resolution enhances the modeled eddy heat transport while leaving its structure generally unchanged, as was suggested by Beckmann et al. (1994). Over the World Ocean, the eddy heat transport is a significant contributor to the total time-mean, particularly on either side of the equator, where there is a southward eddy heat transport of 0.9 PW at 5°N and 0.5 PW northward eddy heat transport at 5°S. The large convergent eddy heat transport at the equator is consistent with observa-

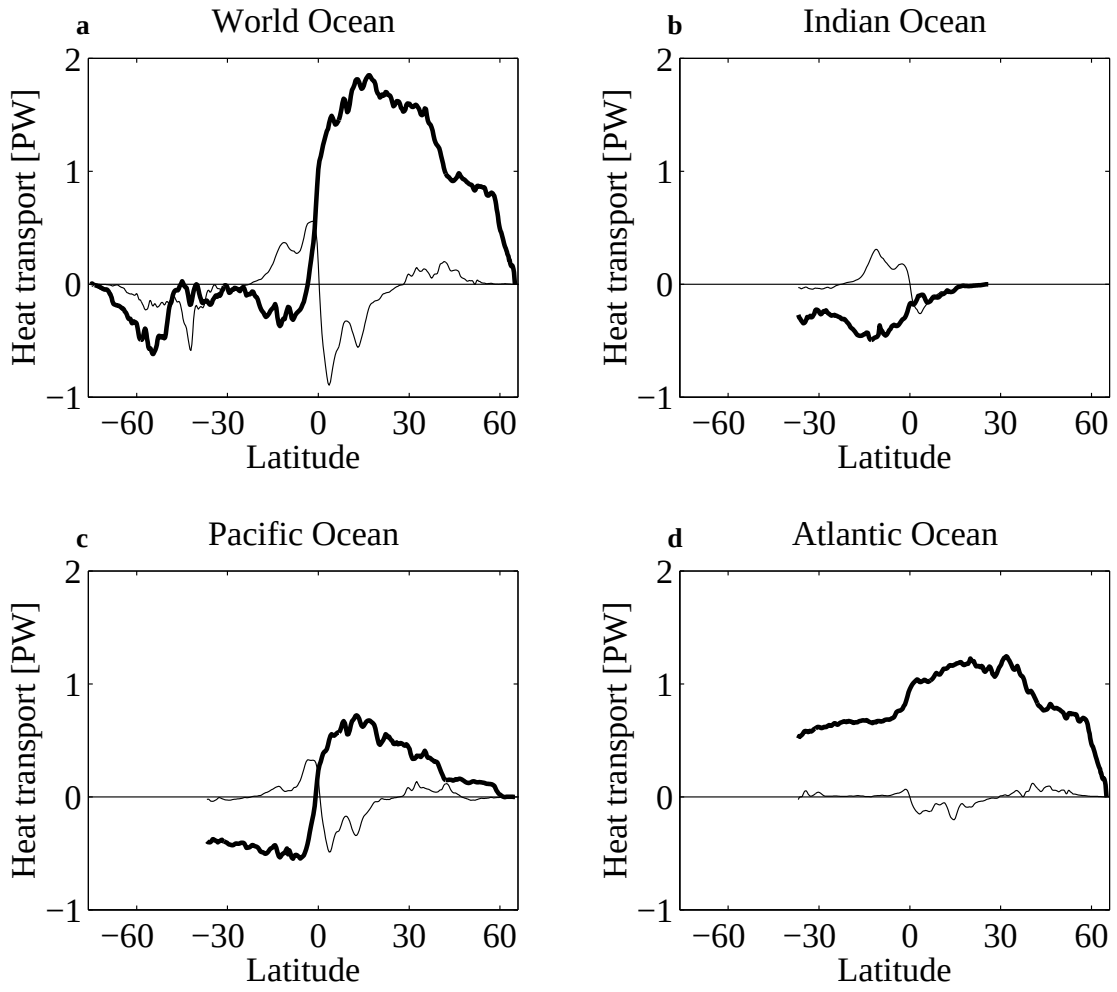

Figure 1. Zonally integrated total time-mean northward heat transport (heavy line) and eddy rectified portion of the total (thin line) for (a) the World Ocean, (b) the Indian Ocean, (c) the Pacific Ocean and (d) the Atlantic Ocean.

tions from current meter arrays by Bryden and Brady (1989) and Baturin and Niiler (1997) and previous modeling work by Philander and Pacanowski (1986). Farther from the equator there is a second peak in eddy heat transport, which is especially noticeable in the Indian Ocean south of the equator at around 15°S; it will be shown later that this is associated with an area of intense activity in the western half of the Indian Ocean, likely from the intense monsoonal activity there. Another peak is in the Pacific Ocean at 15°N, also concentrated in the western part of the basin. Elsewhere, the eddy transport is large in the Southern Indian Ocean along the Antarctic Circumpolar Current, where approximately 0.6 PW of heat is carried southward by the eddies, which is the same order of magnitude as the observed time-mean heat transport there (Macdonald and Wunsch 1996). Overall, in the northern mid-latitudes, there is a small eddy heat transport of peak amplitude of 0.2 PW for the World Ocean.

Figure 3 shows how the eddy heat transport is distributed over four depth bins; the model surface layer (0–25 m), the near surface (25–985 m), the mid-depths (985–2750 m), and the deep ocean (2750–5200 m). Several features stand out. First, most of the the eddy heat transport is contained in the near surface (0–985 m), suggesting that the dynamics that lead to the eddy heat transport are confined to the upper ocean, in line with previous model results from Böning and Cox (1988). Second, there is a broad scale eddy heat transport over the mid-latitudes of both hemispheres in the surface (0–25 m) layer of order 0.1–0.2 PW, which is associated with a rectification of the Ekman layer variability. Finally, the two deepest depth bins account for very little of the eddy heat transport despite their covering about 75% of the total ocean depth. An exception is the mid-depth range

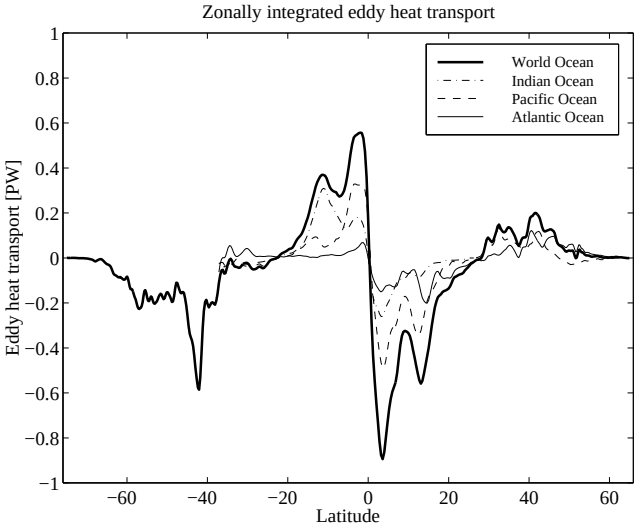

Figure 2. Zonally integrated northward eddy heat transport for World Ocean (heavy line), Indian Ocean (dashed-dotted line), Pacific Ocean (dashed line) and Atlantic Ocean (light solid line).

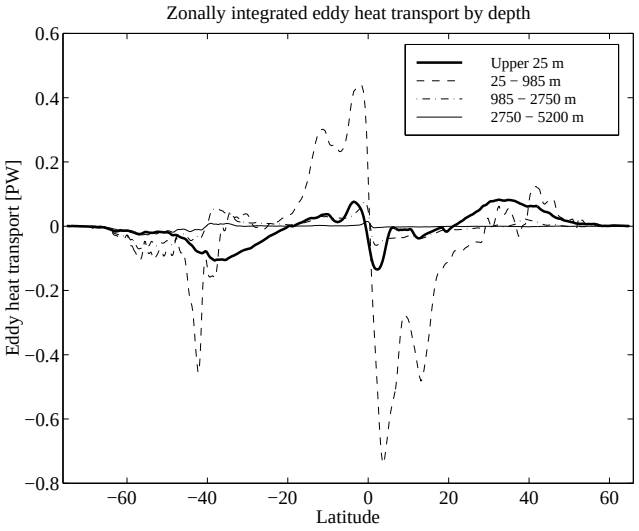

Figure 3. Zonally integrated northward eddy heat transport broken down by depth bin, for surface 25 m (heavy solid line), 25–985 m (dashed line), 985–2750 m (dashed-dotted line) and 2750–5200 m (light solid line).

(985–2750 m) which has a small but significant contribution near the equator. Wunsch (1999) in his quasi-global estimate of eddy heat transports from current meter data also found that the majority of the eddy heat transport was confined to the upper 1000 m.

Finally, we can consider the eddy heat transports due to the different dynamical overturning components. Figure 4 shows the zonal basin integrals of the eddy heat transport for the 4 components of the overturning decomposition in Lee and Marotzke (1998) and Hall and Bryden (1982) (see also Jayne and Marotzke 2001). They are: 1) The contribution to the meridional velocity due to the external mode (or barotropic gyre circulation) flowing over varying topography. Essentially, it is the flow governed by the Sverdrup relation taking into account time dependence, bottom topography and frictional effects. 2) The surface Ekman flow minus its vertical average to represent its barotropic compensation. The Ekman component of velocity, is taken here to be the shear velocity in the four surface levels referenced to velocity at the fifth model level (117.5 m), however, nearly all the Ekman transport takes place in the top level (uppermost 25 m). 3) The zonal-average over the basin of vertical shear flow which is generally associated with thermal wind shear balanced by zonal density gradients, as well as smaller contributions from the ageostrophic shear from frictional and nonlinear effects. 4) Deviations from the zonally-averaged vertical shear flow which is generally associated with baroclinic eddies.

There is an eddy heat transport associated with the Ekman component that is about 0.1 PW in the mid-latitudes and looks remarkably similar to the eddy heat transport in the upper 25 m of the ocean. This distribution suggests two important conclusions: The first is that there is a small, order 0.1–0.2 PW, rectified eddy heat transport due to covarying Ekman layer transports and temperature fluctuations not being fully in quadrature. The second is that the majority of the eddy heat transport is associated with the deviations from the zonal mean in the baroclinic shear term. The confinement of the eddy heat transport to the upper 1000 m and its association with the deviations in the baroclinic shear intimate that baroclinic processes are the dominant process. The barotropic gyre component also contributes strongly to the eddy heat transport in the Antarctic Circumpolar Current, implying that barotropic eddies interacting with topography may play a role there.

3. A meandering jet

So far only the zonal integral of the northward component of the eddy heat transport has been considered; however, the depth-integrated eddy heat transport is a two-dimensional vector quantity in space. Figure 5 shows the depth integrated vector eddy transport for the region of the Gulf Stream off the eastern coast of the United States. This particular region was chosen for its general interest as well as its historical current-meter coverage. While there are obvious model de-

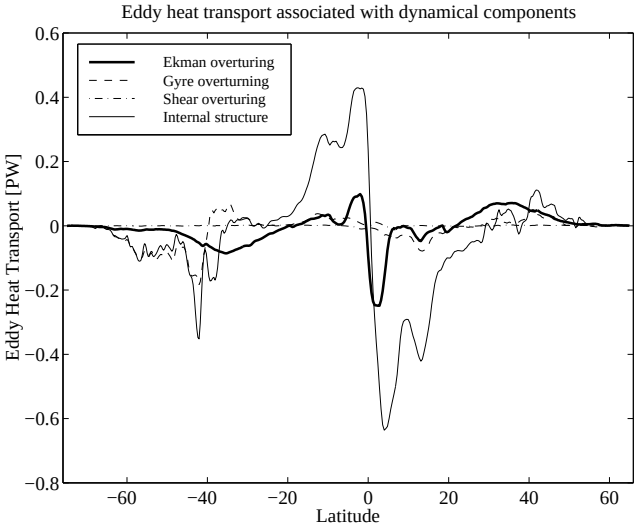

Figure 4. Eddy transport decomposed by dynamical component, for the Ekman overturning (heavy solid line), the gyre component (dashed line), the zonal mean shear (dashed-dotted line) and the eddy component (thin solid line).

ficiencies in this area, notably that the Gulf Stream tends to follow the coast too tightly and it separates too far north of Cape Hatteras, there are some qualitative conclusions that can be drawn by comparing the eddy heat-transport field to observations. The SYNOP arrays which were located in the Gulf Stream at 55°W, discussed by Bower and Hogg (1996), and, at 68°W, analyzed by Cronin and Watts (1996), provide guidance here. Both these studies found significant eastward (downstream) eddy heat transport with small meridional (cross-stream) eddy heat transports, consistent with the overall behavior of the model.

As was discussed by Marshall and Shutts (1981), the eddy heat transport is composed of two different dynamical components; the rotational and the divergent. The rotational component does not contribute to the globally-integrated poleward transport of heat by the oceans, nor does it contribute to the local energy balance, as it transports as much energy into any given region as it does out of the region. The divergent component on the other hand does affect the local heat budget, and therefore is dynamically active. To examine the eddy heat transport in more detail, it must be separated into its two parts in order to examine the divergent component on its own. However, the distribution of the rotational flux and divergent flux must be determined globally, as they cannot be locally separated.

The separation of the divergent and rotational fluxes is done numerically by taking the divergence of the eddy heat transport, then inverting the divergence with a Laplacian in-

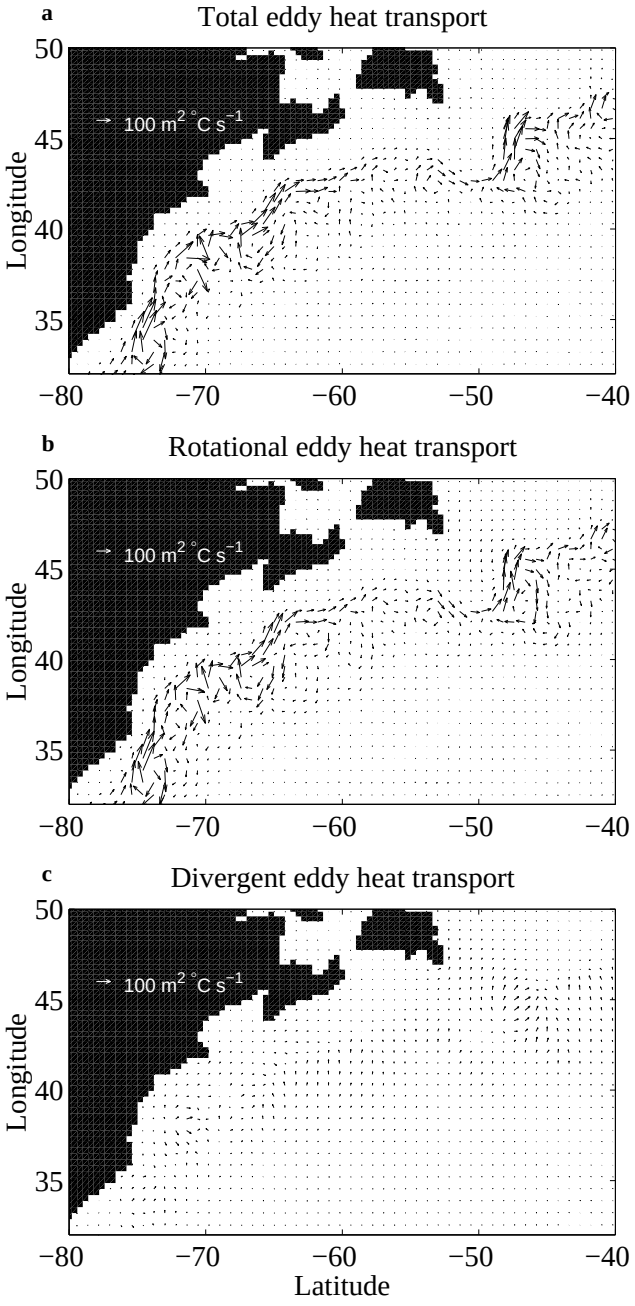

Figure 5. Vector eddy transport for the Gulf Stream region, for (a) the total vector eddy transport, (b) the rotational component and (c) the divergent component. Shown at 1/2 resolution.

verter with Neumann boundary conditions (no heat transport through the lateral boundaries) to find a potential function, and then taking the gradient to recover the vector quantities for the divergent part of the eddy heat transport. A note on

the boundary conditions in appropriate; since the model uses the condition that $u, v = 0$ on the boundaries, it automatically implies that $\mathbf{v}'\theta' = 0$ on the boundaries as well. This does not necessarily mean that the rotational and divergent components must be zero on the boundaries, only their sum need be. However, for their sum to be zero would imply that the rotational part of the eddy heat transport interacts with the divergent part, which should not be so, since the rotational part of the flux does not affect the dynamics. Thus, both the divergent and rotational fluxes should be zero on the boundary to satisfy the boundary condition.

These operations are summarized in the following relations, where $(\overline{\mathbf{v}'\theta})$ is the depth-integrated, eddy heat-transport vector, $(\overline{\mathbf{v}'\theta'})_D$ is the divergent component of the eddy heat transport and $(\overline{\mathbf{v}'\theta'})_R$ is the rotational component:

$$\overline{\mathbf{v}'\theta'} = (\overline{\mathbf{v}'\theta'})_D + (\overline{\mathbf{v}'\theta'})_R \tag{2}$$

$$(\overline{\mathbf{v}'\theta'})_D = \nabla\nabla^{-2}(\nabla \cdot \overline{\mathbf{v}'\theta'}), \tag{3}$$

or

$$\nabla^2\phi = \nabla \cdot \overline{\mathbf{v}'\theta'} \tag{4}$$

and

$$\overline{\mathbf{v}'\theta'}_D = \nabla\phi, \tag{5}$$

since by definition, the divergence of the rotational flux is zero:

$$\nabla \cdot (\overline{\mathbf{v}'\theta'})_R = 0. \tag{6}$$

The rotational component was calculated independently from the following:

$$(\overline{\mathbf{v}'\theta'})_R = \hat{k} \times \nabla\nabla^{-2}(\hat{k} \cdot \nabla \times \overline{\mathbf{v}'\theta'}), \tag{7}$$

where $\hat{k}$ is the unit vector in the vertical direction, or

$$\nabla^2\psi = \hat{k} \cdot \nabla \times \overline{\mathbf{v}'\theta'} \tag{8}$$

and

$$\overline{\mathbf{v}'\theta'}_R = \hat{k} \times \nabla\psi, \tag{9}$$

given that by definition, the curl of the divergent flux is zero:

$$\nabla \times (\overline{\mathbf{v}'\theta'})_D = 0. \tag{10}$$

Returning to Fig. 5, we see that the rotational component dominates the total in the Gulf Stream region. In the divergent component, there appears to be a very weak southward eddy heat transport to the south of the jet axis which is consistent with a down-gradient transport as the meridional temperature gradient reverses sign south of the Gulf Stream in the model, and is consistent with the eddy driving mechanism in the southern recirculation gyre of the Gulf Stream proposed by Bryden (1982).

The strength of the rotational eddy transport compared to the divergent eddy transport requires some explanation. Consider a coherent meandering jet, *e.g.*, the Gulf Stream, the Kuroshio, or the Antarctic Circumpolar Current. In such jets, the meandering mode of the jet can dominate the eddy energy. Indeed, in the Gulf Stream, more than 2/3 of the eddy kinetic and potential energy is due to the meandering of the jet (Rossby 1987; Hogg 1994). If the temperature and velocity have distributions which are set by the following relations, as they would in a quasi-geostrophic jet:

$$u = -\frac{\partial\psi(\xi)}{\partial y} \qquad v = \frac{\partial\psi(\xi)}{\partial x} \qquad \theta = \theta(\xi) \tag{11}$$

$$\psi = \psi_0 \mathcal{F}(\xi) \qquad \theta = \theta_0 \mathcal{F}(\xi) \tag{12}$$

where θ is the temperature, u, v are the eastward and northward velocities given by the streamfunction, ψ. $\mathcal{F}$ is an arbitrary function, and ξ is the spatial and temporal distribution function for the axis of the jet. For example, the "Bickley" jet with a standing wave in it would have a streamfunction with the form:

$$\psi(\xi) = \psi_0 \tanh\left[\frac{y}{L} + \frac{\lambda}{L}\sin\left(\frac{2\pi x}{l}\right)\sin\left(\frac{2\pi t}{\tau}\right)\right] \tag{13}$$

where:

$$\xi = \xi(x,y,t) = \frac{y}{L} + \frac{\lambda}{L}\sin\left(\frac{2\pi x}{l}\right)\sin\left(\frac{2\pi t}{\tau}\right) \tag{14}$$

with the variables x, y, t describing space and time, L being the half-width of the jet, λ the meander amplitude, l the meander wave length and τ the meander period.

The rectified eddy heat transports can then be written as the temporal average over an eddy period:

$$\begin{aligned}\overline{u'\theta'} &= \overline{u\theta} - \overline{u}\,\overline{\theta} = \frac{1}{\tau}\int_0^\tau u\,\theta\,\mathrm{d}t - \frac{1}{\tau^2}\int_0^\tau u\,\mathrm{d}t\int_0^\tau \theta\,\mathrm{d}t \\ \overline{v'\theta'} &= \overline{v\theta} - \overline{v}\,\overline{\theta} = \frac{1}{\tau}\int_0^\tau v\,\theta\,\mathrm{d}t - \frac{1}{\tau^2}\int_0^\tau v\,\mathrm{d}t\int_0^\tau \theta\,\mathrm{d}t \end{aligned} \tag{15}$$

or, in terms of the functional forms:

$$\begin{aligned}\overline{u'\theta'} &= \frac{1}{\tau}\int_0^\tau -\frac{\partial\psi}{\partial y}\,\theta\,\mathrm{d}t - \frac{1}{\tau^2}\int_0^\tau -\frac{\partial\psi}{\partial y}\,\mathrm{d}t\int_0^\tau \theta\,\mathrm{d}t \\ \overline{v'\theta'} &= \frac{1}{\tau}\int_0^\tau \frac{\partial\psi}{\partial x}\,\theta\,\mathrm{d}t - \frac{1}{\tau^2}\int_0^\tau \frac{\partial\psi}{\partial x}\,\mathrm{d}t\int_0^\tau \theta\,\mathrm{d}t \end{aligned} \tag{16}$$

The divergence of the rectified eddy heat flux is given by:

$$\nabla\cdot\overline{\mathbf{v}'\theta'} = \frac{\partial\overline{u'\theta'}}{\partial x} + \frac{\partial\overline{v'\theta'}}{\partial y} \tag{17}$$

which, when written in terms of the functional forms, gives:

$$\begin{aligned}\nabla\cdot\overline{\mathbf{v}'\theta'} = \quad & \frac{\partial}{\partial x}\Big[\frac{1}{\tau}\int_0^\tau -\frac{\partial\psi}{\partial y}\,\theta\,\mathrm{d}t \\ & - \frac{1}{\tau^2}\int_0^\tau -\frac{\partial\psi}{\partial y}\,\mathrm{d}t\int_0^\tau \theta\,\mathrm{d}t\Big] \\ & + \frac{\partial}{\partial y}\Big[\frac{1}{\tau}\int_0^\tau \frac{\partial\psi}{\partial x}\,\theta\,\mathrm{d}t \\ & - \frac{1}{\tau^2}\int_0^\tau \frac{\partial\psi}{\partial x}\,\mathrm{d}t\int_0^\tau \theta\,\mathrm{d}t\Big] \end{aligned} \tag{18}$$

Applying Leibniz's rule and the product rule:

$$\begin{aligned}\nabla\cdot\overline{\mathbf{v}'\theta'} &= \frac{1}{\tau}\int_0^\tau -\frac{\partial^2\psi}{\partial x\partial y}\,\theta\,\mathrm{d}t \\ &+ \frac{1}{\tau}\int_0^\tau -\frac{\partial\psi}{\partial y}\frac{\partial\theta}{\partial x}\,\mathrm{d}t \\ &- \frac{1}{\tau^2}\int_0^\tau -\frac{\partial^2\psi}{\partial x\partial y}\,\mathrm{d}t\int_0^\tau \theta\,\mathrm{d}t \\ &- \frac{1}{\tau^2}\int_0^\tau -\frac{\partial\psi}{\partial y}\,\mathrm{d}t\int_0^\tau \frac{\partial\theta}{\partial x}\,\mathrm{d}t \\ &+ \frac{1}{\tau}\int_0^\tau \frac{\partial^2\psi}{\partial y\partial x}\,\theta\,\mathrm{d}t \\ &+ \frac{1}{\tau}\int_0^\tau \frac{\partial\psi}{\partial x}\frac{\partial\theta}{\partial y}\,\mathrm{d}t \\ &- \frac{1}{\tau^2}\int_0^\tau \frac{\partial^2\psi}{\partial y\partial x}\,\mathrm{d}t\int_0^\tau \theta\,\mathrm{d}t \\ &- \frac{1}{\tau^2}\int_0^\tau \frac{\partial\psi}{\partial x}\,\mathrm{d}t\int_0^\tau \frac{\partial\theta}{\partial y}\,\mathrm{d}t \end{aligned} \tag{19}$$

Canceling like terms leaves:

$$\begin{aligned}\nabla\cdot\overline{\mathbf{v}'\theta'} &= \frac{1}{\tau}\int_0^\tau -\frac{\partial\psi}{\partial y}\frac{\partial\theta}{\partial x}\,\mathrm{d}t \\ &- \frac{1}{\tau^2}\int_0^\tau -\frac{\partial\psi}{\partial y}\,\mathrm{d}t\int_0^\tau \frac{\partial\theta}{\partial x}\,\mathrm{d}t \\ &+ \frac{1}{\tau}\int_0^\tau \frac{\partial\psi}{\partial x}\frac{\partial\theta}{\partial y}\,\mathrm{d}t \\ &- \frac{1}{\tau^2}\int_0^\tau \frac{\partial\psi}{\partial x}\,\mathrm{d}t\int_0^\tau \frac{\partial\theta}{\partial y}\,\mathrm{d}t \end{aligned} \tag{20}$$

Using the chain rule, *i.e.* $\frac{\partial\psi}{\partial x} = \frac{\partial\xi}{\partial x}\frac{\partial\psi}{\partial\xi}$, etc., yields:

$$\begin{aligned}\nabla\cdot\overline{\mathbf{v}'\theta'} &= \frac{1}{\tau}\int_0^\tau -\frac{\partial\xi}{\partial y}\frac{\partial\psi}{\partial\xi}\frac{\partial\xi}{\partial x}\frac{\partial\theta}{\partial\xi}\,\mathrm{d}t \\ &- \frac{1}{\tau^2}\int_0^\tau -\frac{\partial\psi}{\partial y}\,\mathrm{d}t\int_0^\tau \frac{\partial\theta}{\partial x}\,\mathrm{d}t \\ &+ \frac{1}{\tau}\int_0^\tau \frac{\partial\xi}{\partial x}\frac{\partial\psi}{\partial\xi}\frac{\partial\xi}{\partial y}\frac{\partial\theta}{\partial\xi}\,\mathrm{d}t \\ &- \frac{1}{\tau^2}\int_0^\tau \frac{\partial\psi}{\partial x}\,\mathrm{d}t\int_0^\tau \frac{\partial\theta}{\partial y}\,\mathrm{d}t \end{aligned} \tag{21}$$

Canceling the first and third terms:

$$\begin{aligned}\nabla\cdot\overline{\mathbf{v}'\theta'} = \quad & - \frac{1}{\tau^2}\int_0^\tau -\frac{\partial\psi}{\partial y}\,\mathrm{d}t\int_0^\tau \frac{\partial\theta}{\partial x}\,\mathrm{d}t \\ & - \frac{1}{\tau^2}\int_0^\tau \frac{\partial\psi}{\partial x}\,\mathrm{d}t\int_0^\tau \frac{\partial\theta}{\partial y}\,\mathrm{d}t \end{aligned} \tag{22}$$

Expanding the functional forms for the temperature and streamfunction:

$$\begin{aligned}\nabla\cdot\overline{\mathbf{v}'\theta'} &= \frac{\theta_0\psi_0}{\tau^2}\int_0^\tau\frac{\partial\mathcal{F}}{\partial y}\,\mathrm{d}t\int_0^\tau\frac{\partial\mathcal{F}}{\partial x}\,\mathrm{d}t \\ &- \frac{\theta_0\psi_0}{\tau^2}\int_0^\tau\frac{\partial\mathcal{F}}{\partial x}\,\mathrm{d}t\int_0^\tau\frac{\partial\mathcal{F}}{\partial y}\,\mathrm{d}t \\ &= 0. \end{aligned} \tag{23}$$

Therefore, there is no divergent part of the rectified eddy heat transport due to a coherent meandering jet, regardless of its relative functional form and irrespective of its meander mode. All of the rectified eddy heat transport due to a meandering structure is therefore rotational. To illustrate this, consider the eddy heat transport for two examples of meandering. The first is a standing wave pattern in a jet, and the second is a traveling wave structure that grows in amplitude and then decays. The standing wave pattern is given by (14) and is shown in Fig. 6. The meandering jet which has a standing wave in it has an eddy heat transport that is a series of highs and lows. While the temperature gradient is directed in only one direction across the jet, the cross-stream eddy heat transport varies in direction along the jet. Therefore, it can be said that the eddy heat transport is not directly associated with the cross-stream temperature gradient.

The second example is jet structure in which a traveling wave grows and then decays. This was the behavior discussed by Marshall and Shutts (1981). The spatial and temporal form for its meander mode could be given by a function like:

$$\xi(x,y,t) = \frac{y}{L} + \frac{\lambda}{L}e^{-x^2/\Lambda^2}\sin\left(\frac{2\pi x}{l} - \frac{2\pi t}{\tau}\right) \tag{24}$$

As can be seen by comparing Fig. 7 with Fig. 6, despite the jets having very similar instantaneous jet shapes, their eddy statistics are very different. In Fig. 7, the series of highs and lows are replaced by a single dipole. But, again the heat transport is only rotational. Contrasting Fig. 6 and Fig. 7, it can be seen that the rotational component of the eddy transport can make analyses of the eddy heat transport using scattered current meters, as was done by Wunsch (1999), very difficult to interpret.

4. The global distribution of eddy transport

The global picture of the eddy heat transport is now considered. The POCM's total eddy heat transport is shown

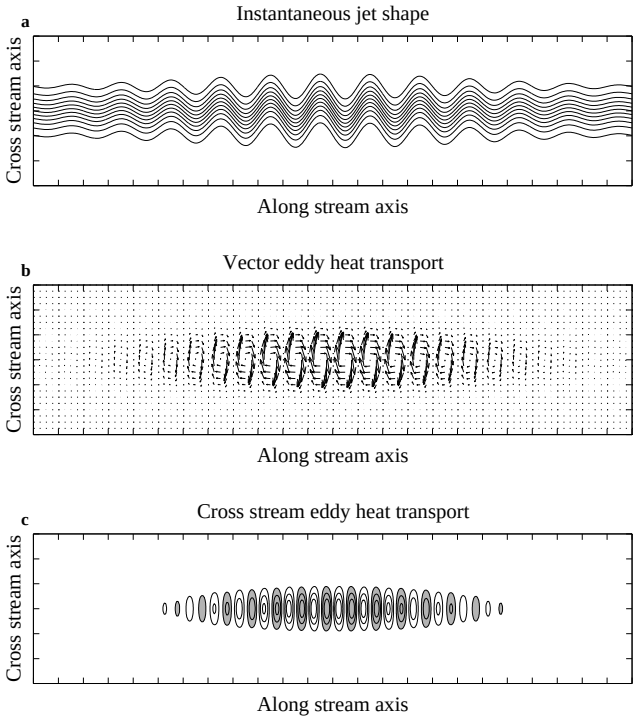

Figure 6. (a) Instantaneous streamfunction and temperature for jet with standing wave pattern in it. (b) Eddy heat transport vectors. (c) Cross-stream heat transport magnitude, black contours indicate heat transport in the positive cross-stream direction, gray-shaded contours indicate opposite direction.

with its rotational and divergent components in Fig. 8a–c. For clarity only the northward component is contoured. The model's eddy heat transport can be compared to an estimate of the eddy heat transport made using an eddy diffusivity derived from altimetry data by Stammer (1998) in Fig. 8d. The zonal basin integrals of the eddy heat transports for POCM and the Stammer (1998) estimates are shown in Fig. 9. The analysis of Stammer (1998) is derived from an eddy transfer of temperature, for which the eddy diffusivity was derived from TOPEX/POSEIDON measurements and combined with a climatological temperature field (Levitus et al. 1994) to compute the eddy transport. This analysis assumes that temperature is fluxed down-gradient by Fickian-like processes. The eddy heat transport is given by:

$$\overline{\mathbf{v}'\theta'} = -\kappa\nabla_h\overline{\theta} \tag{25}$$

where $\overline{\theta}$ is the time-mean temperature from Levitus et al. (1994) climatology averaged over the upper 1000 m. The

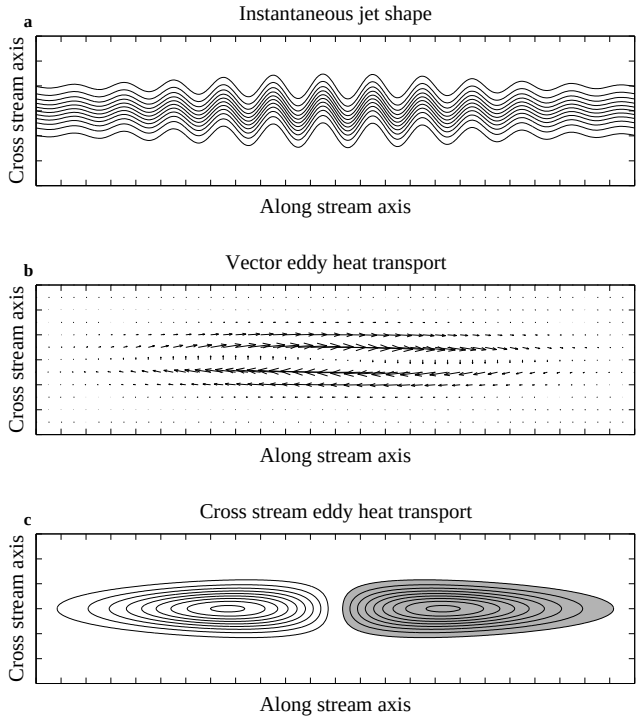

Figure 7. (a) Instantaneous streamfunction for jet with growing and decaying translating waves in it. (b) Eddy heat transport vectors. (c) Cross-stream heat transport magnitude, black contours indicate heat transport in the positive cross-stream direction, gray-shaded contours indicate opposite direction.

eddy transfer coefficient, κ, was estimated from:

$$\kappa(x,y) = 2\ \alpha\ K_E(x,y)\ T_{alt}(x,y). \tag{26}$$

where the eddy kinetic energy, K_E, and the eddy mixing timescale, T_{alt}, were calculated from TOPEX/POSEIDON observations and α, the mixing efficiency, was deduced from current meter observations to be 0.005.

The estimate by Stammer (1998) should be considered to be a calculation of only the divergent eddy heat transport, and as such should be compared to the divergent part of the POCM eddy heat transport. If κ were constant, there would be only a divergent component. However, the rotational part of Stammer (1998) estimate is still minor, since the curl of a diffusive flux is small according the following:

$$\begin{aligned} \hat{k}\cdot\nabla\times\overline{\mathbf{v}'\theta'} &= -\hat{k}\cdot\nabla\times\kappa\nabla\overline{\theta} \\ &= \hat{k}\cdot\kappa\nabla\times\nabla\overline{\theta}+\hat{k}\cdot\nabla\kappa\times\nabla\overline{\theta}. \end{aligned} \tag{27}$$

The first term of the right hand side of (27) is zero by definition, and the second term of (27) is small since $\nabla\kappa$ and $\nabla\overline{\theta}$ tend to be oriented in the same direction, so their cross-product is small. This is opposed to the divergent part of the diffusive flux, given by:

$$\begin{aligned} \nabla\cdot\overline{\mathbf{v}'\theta'} &= -\nabla\cdot\kappa\nabla\overline{\theta} \\ &= \kappa\nabla^2\overline{\theta}+\nabla\kappa\cdot\nabla\overline{\theta}. \end{aligned} \tag{28}$$

where the $\kappa\nabla^2\overline{\theta}$ term dominates since κ and $\nabla^2\overline{\theta}$ are both maximum in magnitude along the baroclinic fronts.

A preliminary examination of the POCM's eddy heat transport compared to Stammer (1998) shows some distinct similarities and differences between the two. First, the POCM shows a convergent eddy heat transport along the equator which is completely lacking in the Stammer (1998) calculation. Second, the Antarctic Circumpolar Current shows a significant southward eddy heat transport in both estimates, though there is some discrepancy in its magnitude. Third, Stammer (1998) found a strong and widespread northward eddy heat transport across both the Gulf Stream and the Kuroshio, that is not observed in the model. Despite all the differences there are some general similarities; in particular the weak eddy heat transports in the centers of the ocean gyres seems to be robust and is supported by the current meter compilation by Wunsch (1999). On a final note, Stammer (1998) does not include the eddy heat transport due to rectification of Ekman layer variability, but it is a small contribution (order 0.1 PW) to the total and could be computed separately from the wind stress and Ekman layer temperature from climatologies.

To understand the differences between the Stammer (1998) estimate of the eddy heat transport and the POCM's eddy heat transport, his method is applied directly to the model output using the time-varying sea-surface height field and time-mean temperature field from the model. If the result of this calculation were to agree well with the model's directly estimated eddy heat transport, then it would indicate that the Stammer (1998) method is a robust way to calculate the eddy heat transport, and would support applying it to the general ocean. If it does not, then it suggests that his method may not correctly predict the eddy transports. Indeed, the resulting estimate (Fig. 8e) is very similar in character to the Stammer (1998) estimate and is very unlike the model's actual eddy heat transport in many parts of the ocean, which implies that the method used by Stammer (1998) to calculate the eddy heat transport is not appropriate. Additionally, this can be considered a test of the model's simulation of the ocean's eddy field. The model, at least qualitatively,

a Total meridional depth integrated eddy heat transport

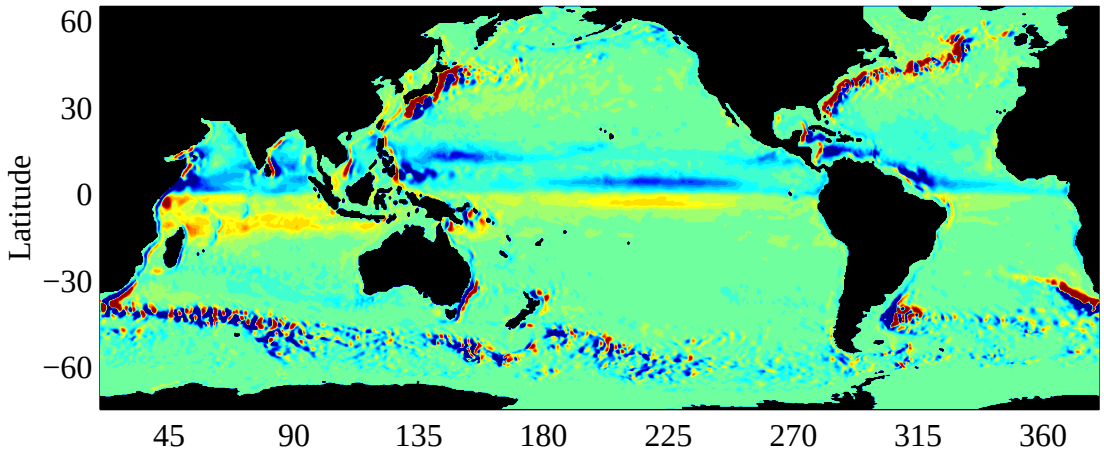

b Rotational meridional depth integrated eddy heat transport

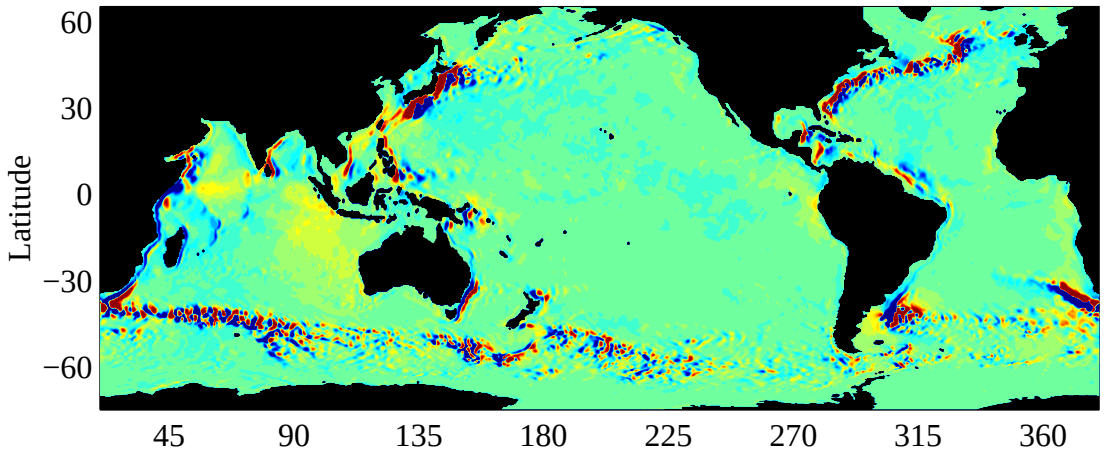

c Divergent meridional depth integrated eddy heat transport

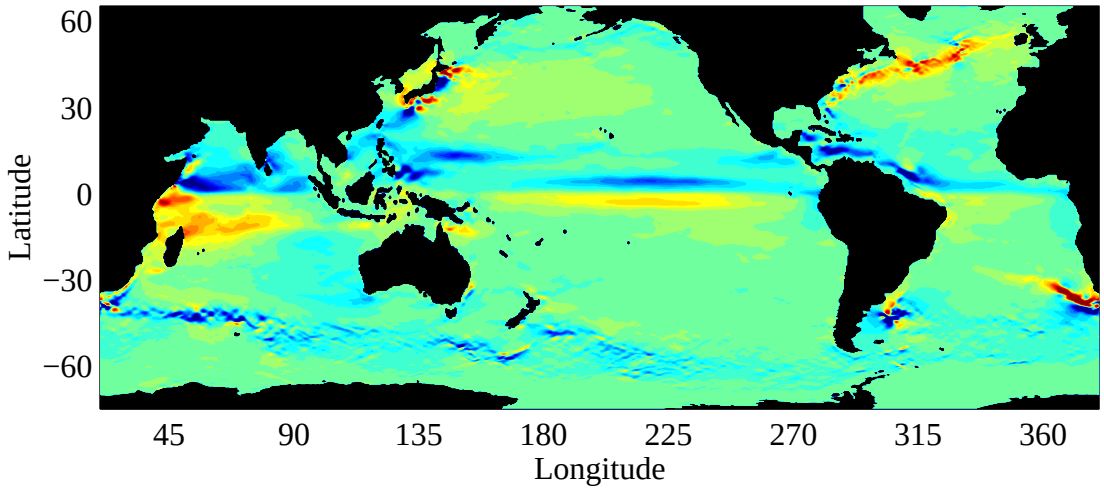

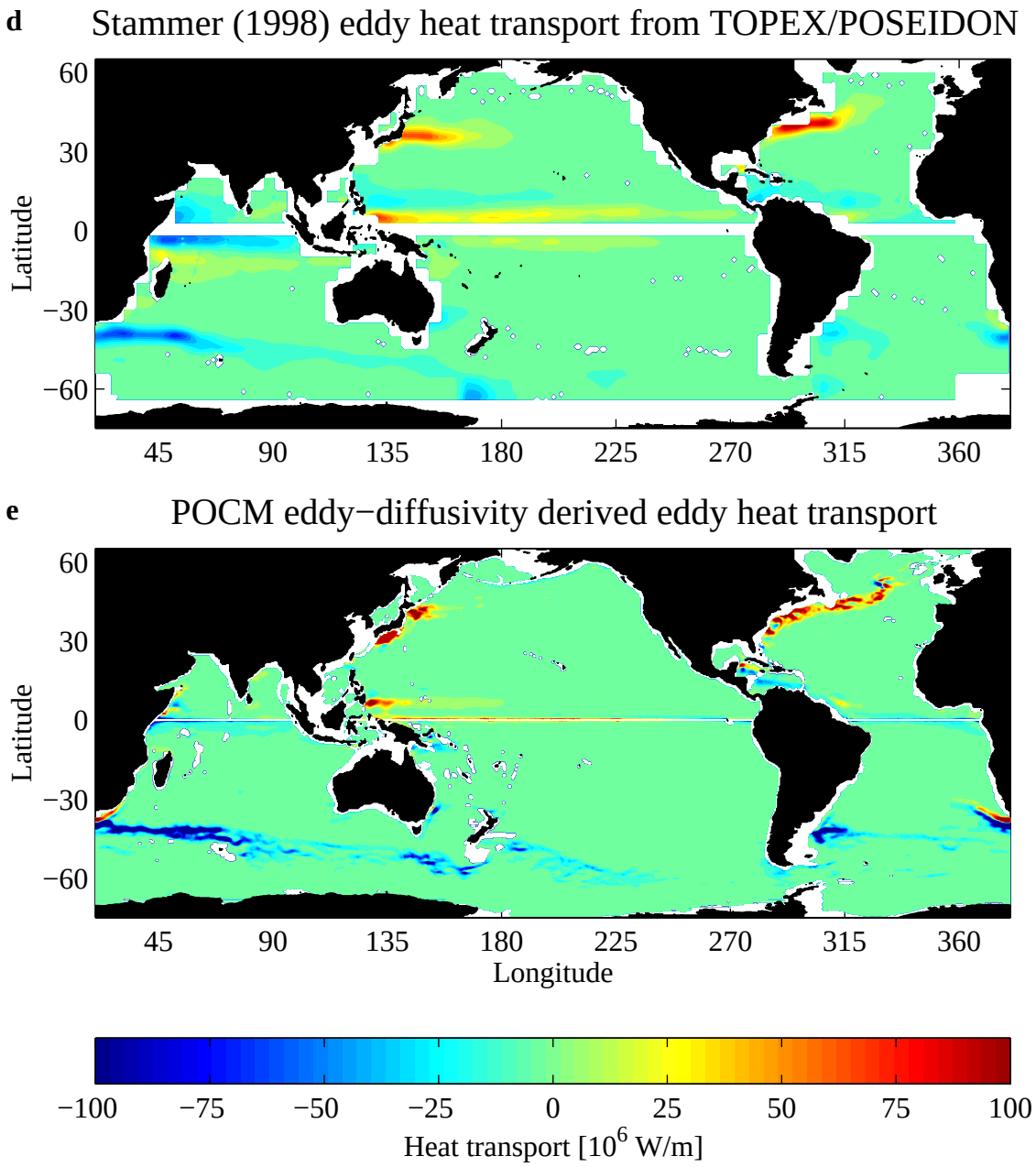

Figure 8. (a) Total, depth integrated, northward eddy heat transport as a function of latitude and longitude. (b) Rotational component of depth integrated eddy heat transport. (c) Divergent component of depth integrated eddy heat transport. (d) Estimate of eddy heat transport by Stammer (1998) using TOPEX/POSEIDON data. (e) Estimate of eddy heat transport using Stammer's (1998) method with POCM. Colorbar extends from -1×10^8 to 1×10^8 W m^{-1}.

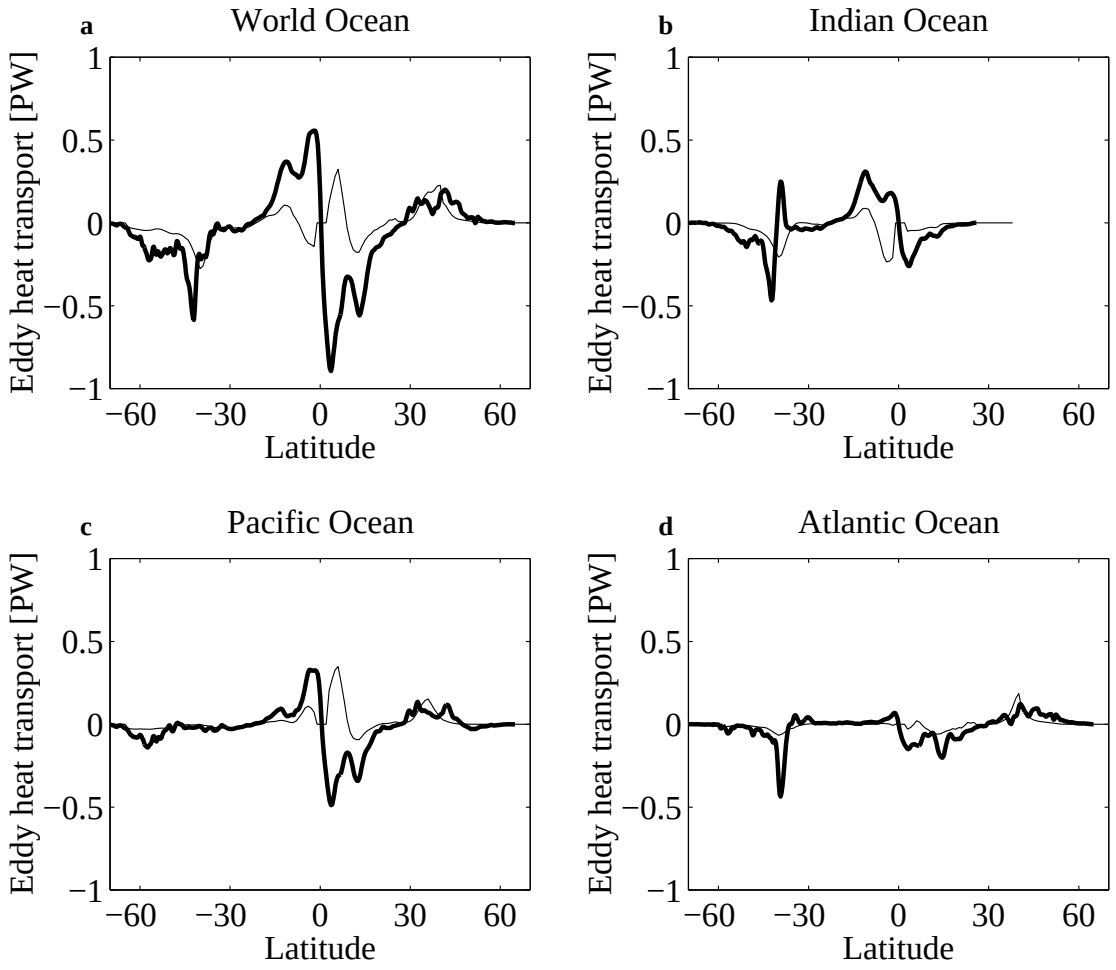

Figure 9. World Ocean for POCM (heavy line) and Stammer (1998) (light line). (b) Same but for Indian Ocean, (c) Pacific Ocean and (d) Atlantic Ocean. The heat transport scale is in petawatts.

appears to be reproducing the large-scale eddy patterns observed by TOPEX/POSEIDON (Stammer et al. 1996), as it gives nearly the same result for the eddy diffusivity derived using method of Stammer (1998). Some possible reasons for the differences in the two eddy heat transport estimates will be discussed below.

There are three regimes to where the model's eddy heat transport will be compared to the Stammer (1998) estimate in detail. The first is in the Southern Ocean. The two estimates of the eddy heat transport in the Antarctic Circumpolar Current (ACC) region are generally consistent, though the model estimate is larger there, 0.6 PW in the POCM versus what Stammer (1998) considers to be a lower bound for the ACC of 0.3 PW. The amplitude of the eddy heat transport across the ACC is consistent with the estimate of 0.45 ± 0.3 PW from de Szoeke and Levine (1981), but is somewhat larger than the values of 0.3 PW from Gordon and Owens (1987) and 0.2 PW from analysis of the Fine Resolution Antarctic Model by Thompson (1993).

The current meter data from the ACC are inconclusive. Bryden (1979) found a significant southward eddy heat transport in the Drake Passage, and, by extrapolation to the rest of the ACC, thought that it was sufficient to balance the atmospheric heat loss to the south of 60°. However, the Bryden (1979) results were not corrected for mooring blow-over which could have over-estimated the eddy heat transport by as much as 20% (Nowlin et al. 1985). Bryden and Heath (1985) measured the ACC west-southwest of New Zealand and found that the eddy heat transport there was too weak to account for the expected loss of heat to the atmosphere, but their measured transports were not statistically significant. It appears from analysis of the POCM that the extrapolation

from either of these two locations is not appropriate, as the strongest southward heat transports in the model are in the the southwestern Indian Ocean sector of the ACC, an area of no current meter coverage. The eddy heat transport is very inhomogeneous, increasing the difficulty of using scattered current meters to extrapolate the eddy heat transport for the rest of the ACC.

The second regime is the area around the western boundary currents. In the Stammer (1998) estimate the Gulf Stream and Kuroshio both have a large northward eddy heat transport that is somewhat smaller in the model. There are, of course, numerous model deficiencies that could play a role in the discrepancies, chief among them being the general weakness of the model temporal and spatial variability, and the failure of the model to reproduce the extension of eddy kinetic energy east of the separation points in the Kuroshio and Gulf Stream as was pointed out by Stammer et al. (1996). In fact, comparing the model's along-stream eddy heat transport to current meter data from the Gulf Stream at 55°W (Bower and Hogg 1996) and 64°W (Cronin and Watts 1996) shows that model under-estimates the eddy heat transport by a factor of about 4. At 55°W, Bower and Hogg (1996) found that the along-stream eddy heat transport was about 150 °C m^2 s^{-1}, while the model only produces about 40 °C m^2 s^{-1} in the axis of the stream at 55°W. Upstream at 68°W, Cronin and Watts (1996) found a stronger eddy heat transport of 900 °C m^2 s^{-1} compared to the model's 200 °C m^2 s^{-1} there.

The lack of strong northward eddy heat transport in the Kuroshio extension and the Gulf Stream recirculation region seen by Stammer (1998) may result from the overall weakness of the model's variability. On the other hand, neither Bower and Hogg (1996) nor Cronin and Watts (1996) observed the widespread strong cross-stream eddy heat transport that Stammer (1998) estimates for the Gulf Stream. Wunsch (1999) found strong southward eddy heat transports in a few locations in both the Gulf Stream and the Kuroshio. In the Kuroshio, he found one location with a southward eddy heat transport of 190 °C m^2 s^{-1}, compared to a weaker, but still southward eddy heat transport of 70 °C m^2 s^{-1} in POCM. These southward heat transports are simply not seen in the Stammer (1998) estimate. However, as was argued in the previous section, it is difficult to know exactly what the current-meter observations are showing in the meandering jets, given the dominance of the rotational eddy heat transports.

The third area is the equatorial region where the model shows a convergent eddy heat transport along the equator in all three of the ocean basins, which is different from the southward eddy transport along the equator in the Indian Ocean and the northward transport in the Pacific Ocean estimated in Stammer (1998). In the equatorial region the POCM is thought to simulate the ocean well, and the convergent eddy heat transport along the equator is supported by previous modeling studies (*i.e.* Semtner and Holland 1980; Cox 1980; Philander and Pacanowski 1986).

The POCM's eddy heat transport in the Equatorial Pacific is consistent with the observational evidence from the region. The POCM finds a convergent eddy heat transport along the equator of 190 W m^{-2} over the region between 110°W and 140°W. Using data from current meters, Bryden and Brady (1989) found a convergent eddy heat transport along the equator between 110°W and 152°W of about 245 W m^{-2}. Two studies using drifters also found a convergent eddy heat transport along the equator of 180 W m^{-2} between 105°W and 120°W (Hansen and Paul 1984), and 100 W m^{-2} between 110°W and 140°W (Baturin and Niiler 1997). So the model appears to be within the range of eddy heat convergence suggested from the observational work. All three of the observational studies, as well as the modeling studies mentioned above, pointed to the importance of tropical instability waves as the energetic fluctuations responsible for the convergent heat transport. These waves have a wavelength of about 1000 km (well resolved by the model's resolution) and periods of 3–4 weeks. They occur within about 5° of the equator and derive their energy from the barotropic velocity shear between the South Equatorial Current and the North Equatorial Countercurrent.

Some resolution to the discrepancies between the Stammer (1998) estimate and the model's directly calculated eddy heat transport is required. The disparity of the results, particularly in the equatorial regions suggests that eddy heat transports from the POCM and mixing length arguments are not just quantitatively different, but qualitatively different as well. We have briefly mentioned one case where Stammer's (1998) method fails, namely in the western boundary currents, where the rotational flux dominates and obscures the divergent flux. Another way of examining why the method of Stammer (1998) may fail is to examine the baroclinic energy conversion term from the turbulent energy equation, which has the following form:

$$-\frac{g}{|\partial\overline{\rho}/\partial z|}\left(\overline{u'\rho'}\,\frac{\partial\overline{\rho}}{\partial x}+\overline{v'\rho'}\,\frac{\partial\overline{\rho}}{\partial y}\right), \tag{29}$$

and is a measure of the conversion of eddy potential energy to other energies such as eddy kinetic energy, mean flow potential energy and mean flow kinetic energy. Where this quantity is negative there is a conversion of energy from the mean flow to the eddy potential energy and where it is positive there is a conversion of energy from the eddy potential energy back to the mean flow. If the effects of salinity are

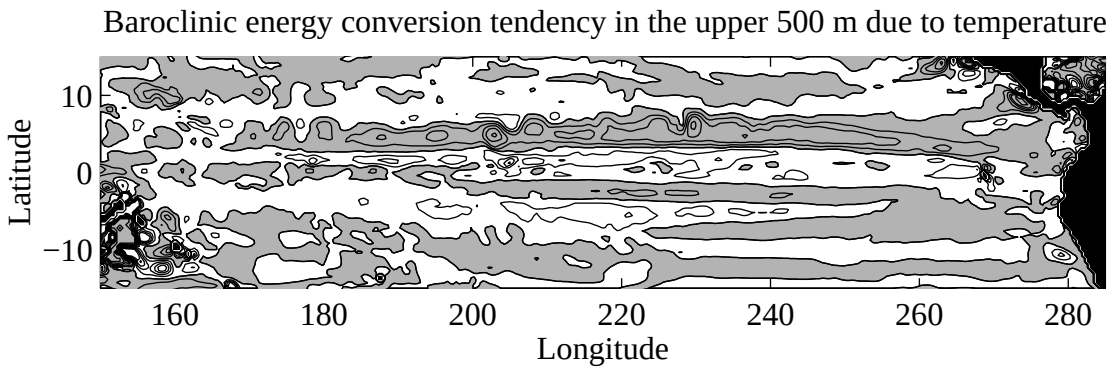

Figure 10. Eddy potential energy conversion tendency due to temperature, estimated by the depth integral of $\overline{\mathbf{v}'\theta'} \cdot \nabla\overline{\theta}$ over the upper 500 meters. The contour interval is 0.001 $^{\circ}$C^2 m s^{-1}, with gray-shaded contours indicate negative values. Negative values correspond to a conversion of mean flow energy to eddy potential energy to the mean flow energy.

neglected and the stratification is reasonably constant over the depth range of interest, as was assumed by Hansen and Paul (1984), then the tendency of the baroclinic energy conversion due to temperature can be approximated by:

$$\overline{u'\theta'}\frac{\partial\overline{\theta}}{\partial x} + \overline{v'\theta'}\frac{\partial\overline{\theta}}{\partial y}. \tag{30}$$

If the method of Stammer (1998) were used to calculate the eddy heat transport then (30) would assume the form:

$$-\kappa|\nabla\overline{\theta}|^2. \tag{31}$$

Hence, using the Stammer (1998) argument, the conversion of eddy potential energy would always be negative since both κ and $|\nabla\overline{\theta}|^2$ are positive, so there would always be a net conversion from the mean-flow's energy to eddy potential energy. However, Hansen and Paul (1984) found positive values for the conversion of eddy potential energy due to temperature south of the equator in the Pacific Ocean, indicating a conversion of energy back from the eddy field to the mean flow there. In the POCM the values of $\overline{\mathbf{v}'\theta'} \cdot \nabla\overline{\theta}$ are consistent with measurements of Hansen and Paul (1984). In particular, they are of the same magnitude, and are negative north of the equator and, more importantly, positive south of the equator (Fig. 10). These positive values indicate that there is a tendency to take energy from the eddy potential energy field and give it back to the mean flow there. This is indicative of an up-gradient transport of temperature and is consistent with the findings of Baturin and Niiler (1997) who concluded from their drifter data that a simple down-gradient temperature flux would not work in the Equatorial Pacific since the eddy coefficient of diffusion changed sign depending on location. They went on to state that climate models would need to explicitly resolve tropical instability waves in order to represent their effects. Bryden and Brady (1989) reached similar conclusions from their current-meter observations.

The conversion of eddy potential energy may then provide a diagnostic to test when and where eddy parameterizations based on down-gradient fluxes will fail in the ocean; they will fail where there is a baroclinic energy conversion from the eddy field to the mean flow. In essence, the eddy parameterization by Stammer (1998) fails to work in the model for the same reason it probably fails to work in the ocean; there are regions in the ocean where the eddy heat transport is up-gradient associated with a net conversion of energy from the eddy field to the mean flow. While it would be gratifying to find a unified argument why the mixing length scalings fail in some locations and work elsewhere, it appears as of now that they may fail for different reasons. In the western boundary currents, the meandering jet gives a large apparent eddy diffusivity, even though there is not necessarily any mixing taking place. In the equatorial regions the apparent up-gradient transport of temperature by the tropical instability waves plays a significant dynamical role. It should be noted that these two regimes are both places where there are narrow, barotropically-unstable jets, and the solution to the problem may ultimately come from including those dynamics in the parameterization. In the Antarctic Circumpolar Current, in contrast to these other two regimes, baroclinic instability is dominant and the parameterization gives a consistent estimate, however, it certainly remains possible that they agree for reasons of pure chance.

5. Frequency distribution

One final analysis can be made of the rectified eddy heat transport, that is, a decomposition in the frequency domain. The contribution to the time-mean heat transport by rectification of time-varying processes can be thought of as the integral in the frequency domain of the cospectra of the temperature and velocity (*e.g.,* Bryden 1979):

$$\begin{aligned}\overline{v'\theta'} &= \frac{1}{\tau}\int_{-H}^{0}\int [v'(t,z)\ \theta'(t,z)]\,\mathrm{d}t\,\mathrm{d}z \\ &= \frac{1}{\tau}\int_{-H}^{0}\int \mathrm{Real}[\hat{v}(f,z)\ \hat{\theta}^{*}(f,z)]\,\mathrm{d}f\,\mathrm{d}z. \quad (32)\end{aligned}$$

where $\hat{v}(f)$ is the Fourier transform of the velocity time-series, $v'(t)$, and $\hat{\theta}^{*}(f)$ is the complex conjugate of the Fourier transform of the temperature time-series, $\theta'(t)$, and τ is the averaging period.

The cospectra for 4 locations are shown in Fig. 11. The cospectra have been multiplied by the frequency to emphasize the higher frequency range while making sure that the area under the curve is proportional to the heat transport at that frequency. The frequency distribution of the eddy heat transport is widely variable around the global ocean. In the equatorial Pacific, most of the covariance is in the frequency band of 20 – 50 days, consistent with the hypothesis that the tropical instability waves by Hansen and Paul (1984) and Baturin and Niiler (1997) are responsible for the eddy heat transport there. This is to be contrasted with the tropical Indian Ocean location where the covariance is spread over a much broader range of frequencies from 50 – 500 days, and the Kuroshio where periods around the annual cycle appear to dominate. The ACC location, which is south of Madagascar, is perhaps the most difficult to understand. The cospectra there are noisy, which could be due to the variability from the strong meandering current there, and it appears that even very long fluctuations with periods of a 1000 days contribute significantly. One of the weaknesses of this analysis is its inability to distinguish the rotational eddy heat transport from the divergent eddy heat transport which is strong in the ACC. Surely the two must have different frequency distribution, but it is not obvious how to compute the separated cospectra.

6. Discussion and conclusions

Globally, internal oceanic instabilities (eddies) play only a minor role in the time-dependent heat transport (Jayne and Marotzke 2001). They do, however, contribute to the time-mean heat transport in a number of locations. The rectified eddy heat transport was examined in a number of ways. The interiors of the ocean gyres have little eddy heat transport in agreement with analyses of current meter data (Wunsch 1999) and an estimate derived from mixing length arguments (Stammer 1998). The most significant eddy heat transport activity was found in western boundary currents, equatorial regions, and the Antarctic Circumpolar Current. For zonal averages the eddy heat transport makes a significant contribution to the total time-mean heat transport in the tropics and the Antarctic Circumpolar Current. There is a global zonally-integrated eddy heat transport of about 0.2 PW at its maximum due to rectification effects in the Ekman layer and the majority of the eddy heat transport is concentrated in the upper 1000 m of ocean depth.

The POCM's eddy heat transport differs from the estimate constructed by Stammer (1998) from a mixing length argument using altimetry data and a temperature climatology. That method was tested by applying it to the model fields and it was shown that it failed to reproduce the model's directly computed heat transport, bringing into question the validity of the eddy parameterization. In the western boundary currents it was found that there is a large rotational component to the eddy heat transport which results from the meandering of the jets and that it obscures the dynamically important divergent component. An analytical argument shows that for a coherent meandering jet there can be a large rotational eddy heat transport, which is not necessarily down-gradient. This rotational eddy heat transport may make analyses of scattered current-meter records difficult to interpret. Furthermore, the meandering jet has associated with it high levels of eddy kinetic energy which using the Stammer (1998) method would imply high levels of eddy diffusion where none necessarily exist.

Along the equator the rotational component is weak, but there is a convergent eddy heat transport which comes from tropical instability waves with periods from 20–50 days, in agreement with results from current-meter observations (Bryden and Brady 1989), mixed-layer drifters (Hansen and Paul 1984; Baturin and Niiler 1997) and previous modeling work (Semtner and Holland 1980; Cox 1980; Philander and Pacanowski 1986). In some locations the eddy heat transport is up-gradient and is associated with areas of conversion of eddy potential energy to the mean flow energy. In the Antarctic Circumpolar Current region, the model's eddy heat transport agrees well with the estimate by Stammer (1998) possibly because baroclinic instability dominates there. Finally, in the interiors of the gyres the eddy heat transport is very weak and the mixing length argument (Stammer 1998), the evidence from current meters (Wunsch 1999) and the model are all in unanimous agreement that the eddy transports are small there. These results suggest that these analyses should be repeated with higher resolution (and presum-

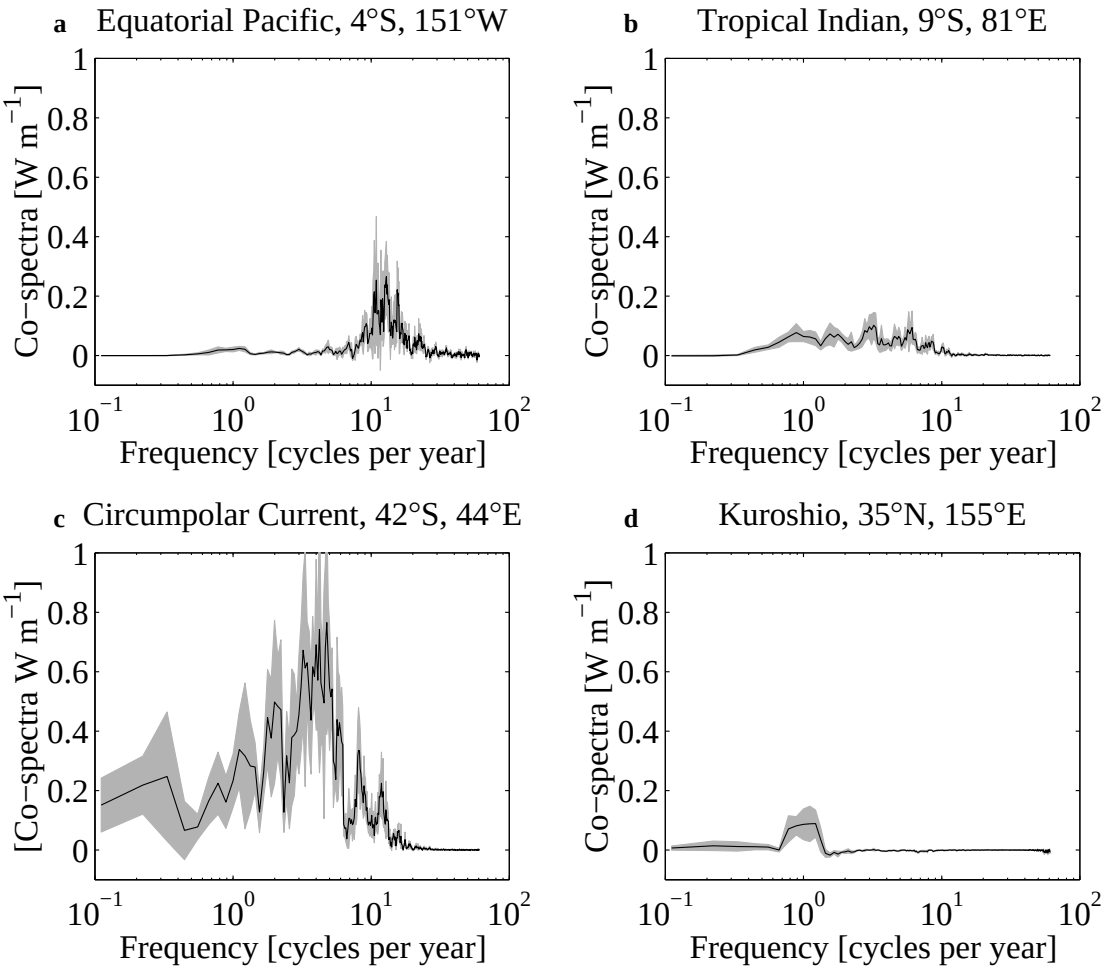

Figure 11. Cospectra of temperature and velocity at 4 selected locations: (a) Equatorial Pacific Ocean, (b) Tropical Indian Ocean, (c) Antarctic Circumpolar Current, and (d) the Kuroshio Current.

ably, more realistic) models in the future when the become available. It also suggests that more work needs to be done on eddy dynamics and their parameterization.

Acknowledgments. Funding for this research came from the Department of Defense under a National Defense Science and Engineering Graduate Fellowship (SRJ), from the National Science Foundation, the American Automobile Manufacturers Association, and the Tokyo Electric Power Company through the TEPCO/MIT Environmental Research Program. The computational resources for this work were provided by the National Center for Atmospheric Research, which is supported by the National Science Foundation. Special thanks are owed to Robin Tokmakian and Bert Semtner from the Naval Postgraduate School, who generously provided their numerical model output. We are also grateful to Nelson Hogg, Detlef Stammer and Carl Wunsch for helpful discussions. This is a contribution to the World Ocean Circulation Experiment.

References

Baturin, N. G. and P. P. Niiler, 1997: Effects of instability waves in the mixed layer of the equatorial Pacific. *J. Geophys. Res.*, **102**, 27,771–27,793.

Beckmann, A., C. W. Böning, C. Köberle and J. Willebrand, 1994: Effects of increased horizontal resolution in a simulation of the North Atlantic Ocean. *J. Phys. Oceanogr.*, **24**, 326–344.

Böning, C. W. and M. D. Cox, 1988: Particle dispersion and mixing of conservative properties in an eddy-resolving model. *J. Phys. Oceanogr.*, **18**, 320–338.

Böning, C. W., W. R. Holland, F. O. Bryan, G. Danabasoglu and J. C. McWilliams, 1995: An overlooked problem in model simulations of the thermohaline circulation and heat transport in the Atlantic Ocean. *J. Climate*, **8**, 515–523.

Bower, A. S. and N. G. Hogg, 1996: Structure of the Gulf Stream and its recirculations at 55° W. *J. Phys. Oceanogr.*, **26**, 1002–1022.

Bryden, H. L., 1979: Poleward heat flux and conversion of available potential energy in Drake Passage. *J. Mar. Res.*, **37**, 1–22.

Bryden, H. L., 1982: Sources of eddy energy in the Gulf-Stream recirculation region. *J. Mar. Res.*, **40**, 1047–1068.

Bryden, H. L. and E. C. Brady, 1989: Eddy momentum and heat fluxes and their effects on the circulation of the equatorial pacific ocean. *J. Mar. Res.*, **47**, 55–79.

Bryden, H. L. and R. A. Heath, 1985: Energetic eddies at the northern edge of the Antarctic Circumpolar Current in the Southwest Pacific. *Prog. Oceanog.*, **14**, 65–87.

Cox, M. D., 1980: Generation and propagation of 30-day waves in a numerical model of the Pacific. *J. Phys. Oceanogr.*, **10**, 1168–1186.

Cox, M. D., 1985: An eddy-resolving numerical model of the ventilated thermocline. *J. Phys. Oceanogr.*, **15**, 1312–1324.

Cronin, M. and D. R. Watts, 1996: Eddy-mean flow interaction in the Gulf Stream at 68° W. Part I: Eddy energetics. *J. Phys. Oceanogr.*, **26**, 2107–2131.

Danabasoglu, G., J. C. McWilliams and P. R. Gent, 1994: The role of mesoscale tracer transports in the global ocean circulation. *Science*, **264**, 1123–1126.

de Szoeke, R. A. and M. D. Levine, 1981: The advective flux of heat by mean geostrophic motions in the Southern Ocean. *Deep-Sea Res.*, **28A**, 1057–1085.

Gent, P. R. and J. C. McWilliams, 1990: Isopycnal mixing in ocean circulation models. *J. Phys. Oceanogr.*, **20**, 150–155.

Gordon, A. L. and W. B. Owens, 1987: Polar oceans. *Rev. Geophys.*, **25**, 227–233.

Griffies, S. M., 1998: The Gent-McWilliams skew flux. *J. Phys. Oceanogr.*, **28**, 831–841.

Hall, M. M. and H. L. Bryden, 1982: Direct estimates and mechanisms of ocean heat transport. *Deep-Sea Res.*, **29**, 339–359.

Hansen, D. V. and C. A. Paul, 1984: Genesis and effects of long waves in the Equatorial Pacific. *J. Geophys. Res.*, **89**, 10,431–10,440.

Hogg, N. G., 1994: Observations of gulf stream meander-induced disturbances. *J. Phys. Oceanogr.*, **24**, 2534–2545.

Holloway, G., 1992: Representing topographic stress for large-scale ocean models. *J. Phys. Oceanogr.*, **22**, 1033–1046.

Jayne, S. R. and J. Marotzke, 2001: The dynamics of ocean heat transport variability. *Rev. Geophys.*, in press.

Kushner, P. J. and I. M. Held, 1998: A test, using atmospheric data, of a method for estimating oceanic eddy diffusivity. *Geophys. Res. Lett.*, **25**, 4213–4216.

Lee, T. and J. Marotzke, 1998: Seasonal cycles of meridional overturning and heat transport of the Indian Ocean. *J. Phys. Oceanogr.*, **28**, 923–943.

Levitus, S., R. Burgett and T. Boyer, 1994: *World Ocean atlas 1994, vol. 3, Salinity, and vol. 4, Temperature, NOAA Atlas NESDIS 3 & 4*. U.S. Department of Commerce, Washington, D.C.

Macdonald, A. M. and C. Wunsch, 1996: An estimate of global ocean circulation and heat fluxes. *Nature*, **382**, 436–439.

Marshall, J. and G. Shutts, 1981: A note on rotational and divergent eddy fluxes. *J. Phys. Oceanogr.*, **11**, 1677–1680.

McCann, M. P., A. J. Semtner and R. M. Chervin, 1994: Transports and budgets of volume, heat, and salt from a global eddy-resolving ocean model. *Clim. Dyn.*, **10**, 59–80.

McClean, J. L., A. J. Semtner and V. Zlotnicki, 1997: Comparisons of mesoscale variability in the Semtner-Chervin 1/4° model, the Los Alamos Parallel Ocean Program 1/6° model, and TOPEX/POSEIDON data. *J. Geophys. Res.*, **102**, 25,203–25,226.

Nowlin, W. D., S. J. Worley and T. Whitworth, 1985: Methods for making point estimates of eddy heat flux as applied to the Antarctic Circumpolar Current. *J. Geophys. Res.*, **90**, 3305–3324.

Philander, S. G. H. and R. C. Pacanowski, 1986: The mass and heat budget in a model of the Tropical Atlantic Ocean. *J. Geophys. Res.*, **91**, 14,212–14,220.

Rix, N. H. and J. Willebrand, 1996: Parameterization of mesoscale eddies as inferred from a high-resolution circulation model. *J. Phys. Oceanogr.*, **26**, 2281–2285.

Rossby, T., 1987: On the energetics of the Gulf Stream at 73W. *J. Mar. Res.*, **45**, 59–82.

Semtner, A. J. and R. M. Chervin, 1992: Ocean general circulation from a global eddy-resolving model. *J. Geophys. Res.*, **97**, 5493–5550.

Semtner, A. J. and W. R. Holland, 1980: Numerical simulation of equatorial ocean circulation. Part I: A basic case in turbulent equilibrium. *J. Phys. Oceanogr.*, **10**, 667–693.

Stammer, D., 1998: On eddy characteristics, eddy transports, and mean flow properties. *J. Phys. Oceanogr.*, **28**, 727–739.

Stammer, D., R. Tokmakian, A. J. Semtner and C. Wunsch, 1996: How well does a 1/4° global circulation model simulate large-scale oceanic observations? *J. Geophys. Res.*, **101**, 25,779–25,811.

Thompson, S. R., 1993: Estimation of the transport of heat in the Southern Ocean using a fine-resolution numerical model. *J. Phys. Oceanogr.*, **23**, 2493–2497.

Visbeck, M., J. Marshall, T. Haine and M. A. Spall, 1997: On the specification of eddy transfer coefficients in coarse resolution ocean circulation models. *J. Phys. Oceanogr.*, **27**, 381–402.

Wunsch, C., 1999: Where do ocean eddy heat fluxes matter. *J. Geophys. Res.*, **104**, 13,235–13,249.

S. R. Jayne, Department of Physical Oceanography, Woods Hole Oceanographic Institution, MS 21, 360 Woods Hole Road, Woods Hole, MA 02543-1541. (e-mail: surje@alum.mit.edu)

J. Marotzke, School of Ocean and Earth Science, University of Southampton, Southampton Oceanography Centre, European Way, Southampton SO14 3ZH, United Kingdom. (e-mail: Jochem.Marotzke@soc.soton.ac.uk)

Received July 9, 2001